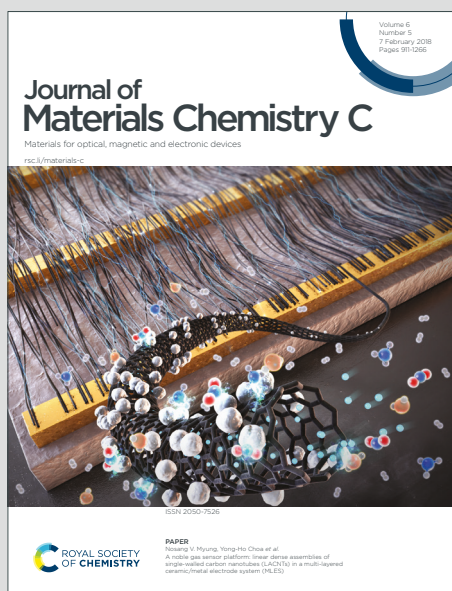


Journal of Materials Chemistry C

Materials for optical, magnetic and electronic devices

Accepted Manuscript

This article can be cited before page numbers have been issued, to do this please use: D. Liu, K. Sun, G. Zhao, J. Wei, J. Duan, M. Xia, W. Jiang and Y. Sun, *J. Mater. Chem. C*, 2019, DOI: 10.1039/C9TC03334C.



This is an Accepted Manuscript, which has been through the Royal Society of Chemistry peer review process and has been accepted for publication.

Accepted Manuscripts are published online shortly after acceptance, before technical editing, formatting and proof reading. Using this free service, authors can make their results available to the community, in citable form, before we publish the edited article. We will replace this Accepted Manuscript with the edited and formatted Advance Article as soon as it is available.

You can find more information about Accepted Manuscripts in the [Information for Authors](#).

Please note that technical editing may introduce minor changes to the text and/or graphics, which may alter content. The journal's standard [Terms & Conditions](#) and the [Ethical guidelines](#) still apply. In no event shall the Royal Society of Chemistry be held responsible for any errors or omissions in this Accepted Manuscript or any consequences arising from the use of any information it contains.

ARTICLE

Spatial separation of TADF sensitizer and fluorescent emitter with core-dendron system to block the energy loss in deep blue organic light-emitting diodesDan Liu,^a Kaiyong Sun,^{ab} Guimin Zhao,^a Jingyi Wei,^a Jiaxin Duan,^a Minghui Xia,^a Wei Jiang*^a and Yueming Sun^aReceived 00th January 20xx,
Accepted 00th January 20xx

DOI: 10.1039/x0xx00000x

An optimized thermally activated delayed fluorescence-(TADF)-sensitized fluorescence (TSF) strategy is proposed to boost the electroluminescent efficiency of the solution-processed deep blue organic light-emitting diodes(OLED). The TADF sensitizer and the fluorescent emitter with core-dendron structure emit mostly by a Förster energy transfer process while the Dexter energy transfer is suppressed by spatial separation. In addition, high-bandgap carbazole terminal substituents are introduced to protect the hyper-fluorescent core by a cascade energy transfer channel. Fluorescent OLEDs based on core-dendron system achieved a deep-blue emission with Commission Internationale de L'Eclairage (CIE) coordinates of (0.15, 0.14) and a high external quantum efficiency of 10.16%. The new TSF system can be used in high efficiency fluorescent OLEDs with 100% exciton utilization, thereby promoting the development of solution-processed blue OLEDs.

1. Introduction

Organic luminescent materials have attracted much attention due to their wide application potential for organic light emitting transistor and sensors, especially organic light-emitting diodes (OLEDs).¹⁻⁶ According to common equation $\eta_{EQE} = (\gamma \times \eta_{\gamma} \times \Phi_{PL}) \times \eta_{out}$, the photoluminescence (PL) quantum yield (Φ_{PL}) of the emitter molecules in film state greatly influences the external quantum efficiency (η_{EQE}) of the OLEDs. However, most fluorescent chromophores have good luminescence properties at low concentrations, but the fluorescence is significantly attenuated at high concentrations or in thin film. This is called aggregation-caused quenching (ACQ).⁷⁻⁹ Highly efficient organic light-emitting materials have been developed to avoid the concentration quenching effect and improve the Φ_{PL} of fluorophores in aggregation states.¹⁰⁻¹⁵ First, the host-guest doping technology can be employed to reduce molecular collisions and further suppress fluorescence quenching by diluting the guest concentration.^{16, 17} Additionally, a series of chemical engineering methods to inhibit the aggregation quenching of luminescent molecules

can be used.^{18,19} Tang et al. designed molecules with aggregation-induced emission (AIE). AIE uniquely increases the emission efficiency in film state compared to solution state.²⁰⁻²⁵ Moreover, the modification of the core chromophores is an important way to optimize the properties of the molecules. Performance of the final material is adjusted by substituting side groups in the core to limit emission quenching.²⁶⁻³² Most emissive materials undergo ACQ and AIE remains difficult. Therefore, core-dendron system (CDS) is a promising route to modify the core chromophores and fabricate solution-processed OLEDs.³³⁻³⁵ The process can be controlled by several parameters. (1) Reducing accumulation of molecules when using bulky side groups to limit emission quenching. (2) Controlling the electron/hole injection and the transport properties, when using dendritic groups with specific electron-donating and electron withdrawing properties. (3) Influencing molecular orientation to increase outcoupling effect. (4) Increasing solubility when introducing alkyl chains.

Many dendrimers have been synthesized with this chemical modification and the performance of the OLED device was improved.³⁶⁻³⁷ However, blue and deep blue dendrimers are still a challenge. Compared to phosphorescent and TADF cores, traditional fluorophores are still ideal blue light materials to develop blue dendrimers, such as anthracene, oligomeric fluorene, bis(styryl) arylene and pyrene derivatives. These molecules have high fluorescence quantum yield and good color purity. By applying CDS and encapsulating with bulky groups, the Φ_{PL} of the fluorescent dendrimers is expected to improve in film state. However, the efficiency of radiative exciton production (η_{γ}) still severely limits η_{EQE} in fluorescent

^a Jiangsu Province Hi-Tech Key Laboratory for Bio-Medical Research, Jiangsu Engineering Laboratory of Smart Carbon-Rich Materials and Device, School of Chemistry and Chemical Engineering, Southeast University, Nanjing, 211189, China
^b School of Chemistry and Chemical Engineering, Yancheng Institute of Technology, Yancheng, Jiangsu 224051, China
Email: jiangw@seu.edu.cn (Wei Jiang)

†Electronic Supplementary Information (ESI) available: Synthesis and characterization details, NMR spectra of compounds, CV curves, TGA curves, XRD spectra, AFM images, photophysical properties and supplementary device performance of PY and PY-Cz. See DOI: 10.1039/x0xx00000x

OLEDs if the 75% of electrically generated excitons formed in the triplet state are not harvested under electrical excitation.^{38, 39} Therefore, many studies were focused on developing singlet-exciton-harvesting fluorescent OLEDs using energy transfer processes to address the 25% internal quantum efficiency threshold.⁴⁰⁻⁴⁶ TADF-sensitized fluorescence (TSF) with traditional fluorescent emitter is a favorable method. A schematic diagram of TSF system is presented in Figure 1. Ideally, all electrically generated singlet- and triplet-excitons of the TADF host are directly transferred into the singlet state of the fluorescent emitter through a Förster energy transfer, which results in efficient radiative decay. However, the triplets of the host may be transferred to the triplet state of the dopant via Dexter transfer and non-radiative decay can occur (Figure 1a). This serious exciton quenching is not only caused by the host-host interaction, but also by host-guest interaction. It inevitably presents in traditional host-guest systems and was usually ignored in the previous studies. Therefore, to optimize THS, the quenching of the triplet excitons must be suppressed, which means Dexter transfer from electron exchange interaction must be prevented.

Herein, we propose a novel TSF system by applying CDS. The short-range Dexter energy transfer can be effectively blocked by increasing the intermolecular distance.⁴⁰ In CDS, the encapsulation of host and guest with the alkyl chain linked dendrons restricts the intermolecular interactions between the emissive cores and makes the molecules more suitable for solution processing.⁴⁷ Because of the increased distance between the cores, potential exciton quenching pathways, such as triplet-triplet annihilation (TTA) and triplet-polaron annihilation (TPA), were blocked, as shown in Figure 1b. Consequently, more triplet excitons can be up-converted for the radiative transition. Based on this energy transfer, we designed and synthesized 2,4,6-tris(3-(6-(9H-carbazol-9-yl)hexyl)-9H-carbazol-9-yl)benzotrile (3CzBN-Cz) TADF molecules as the host and 1,3,6,8-tetrakis(4-((6-(9H-carbazol-9-yl)hexyl)oxy)phenyl)pyrene (PY-Cz) as the fluorescent emitter dopants. We subsequently demonstrate an efficient deep-blue OLED with the maximum external quantum efficiency of 10.16%. For comparison, the corresponding small molecules of 2,4,6-tri(9H-carbazol-9-yl)benzotrile (3CzBN) and 1,3,6,8-tetrakis(4-methoxyphenyl)pyrene (PY) were also

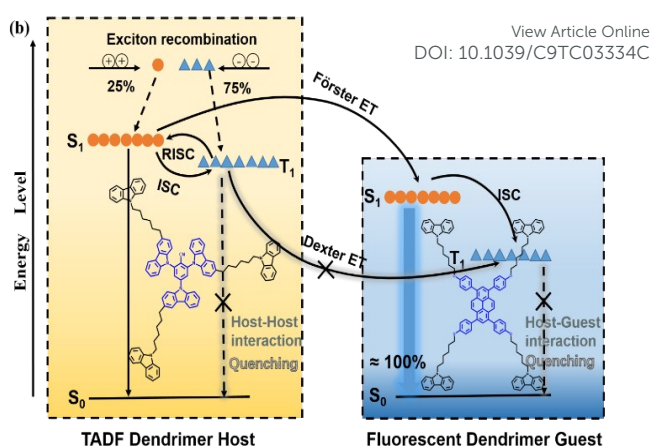


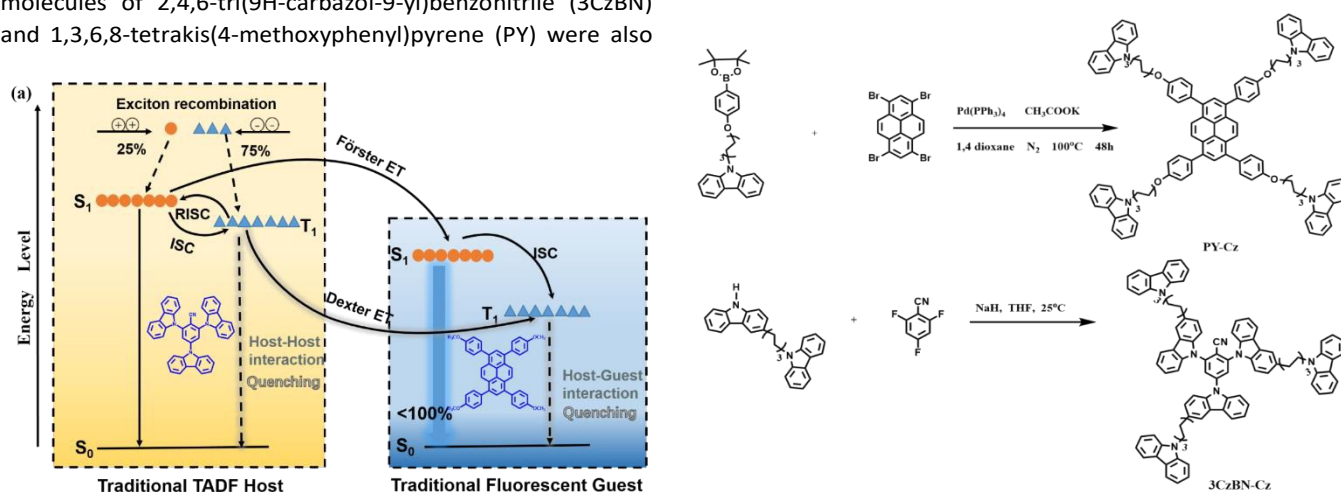
Figure 1 A schematic diagram describing the singlet-exciton-harvesting methods of a) traditional TADF host and traditional fluorescent guest and b) TADF dendrimer host and fluorescent dendrimer guest.

synthesized and studied to highlight the properties of dendrimers.

2. Results and Discussion

2.1 Synthesis and Electrochemical Properties

The synthetic routes of the TADF hosts (3CzBN and 3CzBN-Cz) and the fluorescent guests (PY, PY-Cz) are illustrated in Scheme 1 and in the supplementary information. The fluorescent guests PY and PY-Cz are synthesized through Suzuki aryl-coupling reaction with a yield around 70%. 3CzBN-Cz is synthesized by lithium-halogen exchange reaction and aromatic nucleophilic substitution reactions, that avoid the addition of oxygen and change of the energy gap of the core. Before device fabrication, the target product was separated and purified by silica gel column chromatography and recrystallization. ¹H NMR, ¹³C NMR, mass spectrometry, and elemental analysis were used to confirm the chemical structure of the new compounds. Subsequently, the electrochemical properties of the materials were examined by cyclic voltammetry (CV). The HOMO energy levels of PY, PY-Cz, 3CzBN and 3CzBN-Cz are obtained from the onset of oxidation



Scheme 1. Synthetic route of PY-Cz and 3CzBN-Cz.

(Figure S1). the LUMO energy levels are calculated using the following equation: $E_{\text{LUMO}} = E_{\text{HOMO}} + E_{\text{g}}$. The experimental datas of HOMO and LUMO levels were listed in Table 1, which can match well with the theoretical simulations described later.

2.2 Thermal Properties and Film Forming Abilities

To investigate the influence of their thermal properties on the morphological stability and device performance, thermal gravimetric analysis (TGA) and differential scanning calorimetry (DSC) were carried out at a heating rate of $10\text{ }^{\circ}\text{C min}^{-1}$ under a nitrogen atmosphere. The good thermal stability of dendrimers is indicated by the high decomposition temperatures (Figure S2), and the values of T_{d} corresponding to 5% weight loss are 413°C and 432°C for PY-Cz and 3CzBN-Cz, respectively. These values are consistent with and slightly higher than the ones for small molecules PY (385°C) and 3CzBN (401°C).⁴⁸ Moreover, the values of T_{d} and T_{g} are listed in Table 1. The T_{g} of PY-Cz and 3CzBN-Cz are reduced due to the introduction of flexible chains. The high T_{d} and T_{g} of the dendrimers ensure the high quality film through the wet process and guarantee the long term reliability of the devices.

In addition, the film forming ability of the encapsulated materials is also important for the performance of solution-processed OLEDs. The solution-processed thin films were analysed by atomic force microscope (AFM). Figure S3 indicates that the PY-Cz and 3CzBN-Cz films are greatly smooth with root-mean-square (RMS) values of 0.37 nm and 0.36 nm, which are obviously better than PY (0.49 nm) and 3CzBN (0.50 nm). It can be attributed to the introducing flexible linkers. Furthermore, X-ray diffraction (XRD) analysis of PY, PY-Cz, 3CzBN and 3CzBN-Cz was carried out. The sharp peaks in the diffraction pattern of PY and 3CzBN (Figure S4) prove the existence of crystalline forms. In contrast, no peaks were observed in the XRD spectra of PY-Cz and 3CzBN-Cz, indicating that the flexible chain-linked carbazole units reduce the tendency to crystallize and inhibit molecular aggregation.

2.3 Theoretical Calculations and analysis

The electronic properties of synthesized compounds were investigated using density functional theory (DFT) calculations at the B3LYP level of the theory with 6-31g(d) as the basis set. The LUMOs are localized on the central pyrene core group and partially on the oxyphenylene moieties and the HOMOs are

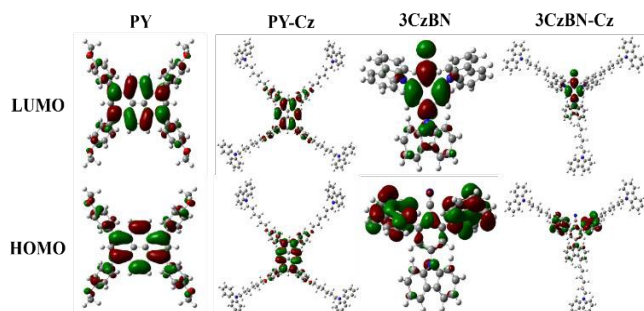


Figure 2 HOMO and LUMO electronic distributions for (a) PY, (b) PY-Cz, (c) 3CzBN and (d) 3CzBN-Cz at the B3LYP/6-31G(d) level.

slightly more delocalized than the LUMOs and have appreciable amplitude on the oxyphenylene moieties, as shown in Figure 2. The large orbital overlap of the HOMO and LUMO are beneficial to the radiative transition. In addition, the HOMOs and LUMOs of 3CzBN-Cz were in agreement with those of 3CzBN. The LUMOs are distributed primarily over the benzonitrile groups, whereas, the HOMOs are delocalized on the carbazole units. 3CzBN and 3CzBN-Cz have a separated HOMO/LUMO distribution and a small energy gap (ΔE_{st}) between the lowest excited singlet state (S_1) and the lowest excited triplet state (T_1), which can produce reverse intersystem crossing (RISC). The theoretical calculated HOMO/LUMO energy levels of PY-Cz and 3CzBN-Cz are $-4.76\text{ eV}/-1.52\text{ eV}$ and $-5.29/-1.98\text{ eV}$ (Table S1). This is similar to the values for PY ($-4.74/-1.48\text{ eV}$) and 3CzBN ($-5.65/-1.92\text{ eV}$). Then the calculated $S_1/T_1/\Delta E_{\text{st}}$ values of PY, PY-Cz, 3CzBN and 3CzBN-Cz are $3.03/1.87/1.16\text{ eV}$, $3.00/1.86/1.14\text{ eV}$, $3.09/2.78/0.31\text{ eV}$ and $3.02/2.81/0.21\text{ eV}$, respectively, which are close to the values estimated from the onset of fluorescence and phosphorescence spectra. Notably, small ΔE_{st} of 3CzBN and 3CzBN-Cz ensures the efficient RISC and, subsequently, efficient TADF emission.

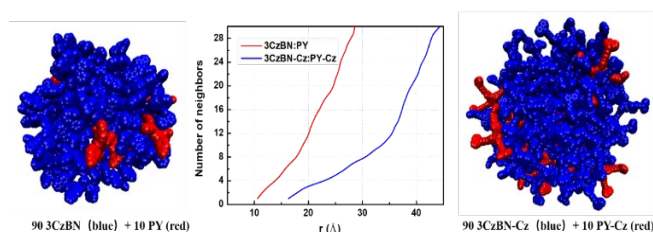


Figure 3 The molecular packing morphologies of mixtures of host and guest by Molclus program simulations and the curve of number of neighbors versus distance of center of mass.

In our optimized TSF system, by blending the fluorescent emitters and the TADF materials, the ΔE_{st} of the host and the PL of the dopant are no longer linked factors and can be optimized separately. In addition, Dexter transfer from T_1 of host to T_1 of guest is suppressed due to the increased distance.⁴⁹ Dexter energy transfer rate constant K_{DEX} is expressed as:

$$K_{\text{Dext}}(\text{exchange}) = K \cdot J_{\text{DA}} \cdot \exp\left(-\frac{2R_{\text{DA}}}{L}\right)$$

Where K is the interaction between related electron orbitals, J_{DA} is the integrated spectral overlap between the donor emission spectrum and acceptor absorption spectrum, R_{DA} is the distance between the donor and the acceptor, and L is the Van der Waals radius between them. According to the equation, K_{DEX} is inversely proportional to the distance of donor and acceptor. And in general, Dexter energy transfer distance (R_{DA}) is small, within $10\text{--}15\text{ \AA}$.⁵⁰ Using this theoretical foundation, we constructed host-guest molecular clusters. More than 100 structures were generated using the Molclus program and adopted as initial structures for the semi-empirical quantum mechanical optimization at PM7 level using MOPAC2016.^{51,52} Then we calculated the distance between the centers of mass of the host and guest.⁵¹ Figure 3 indicates

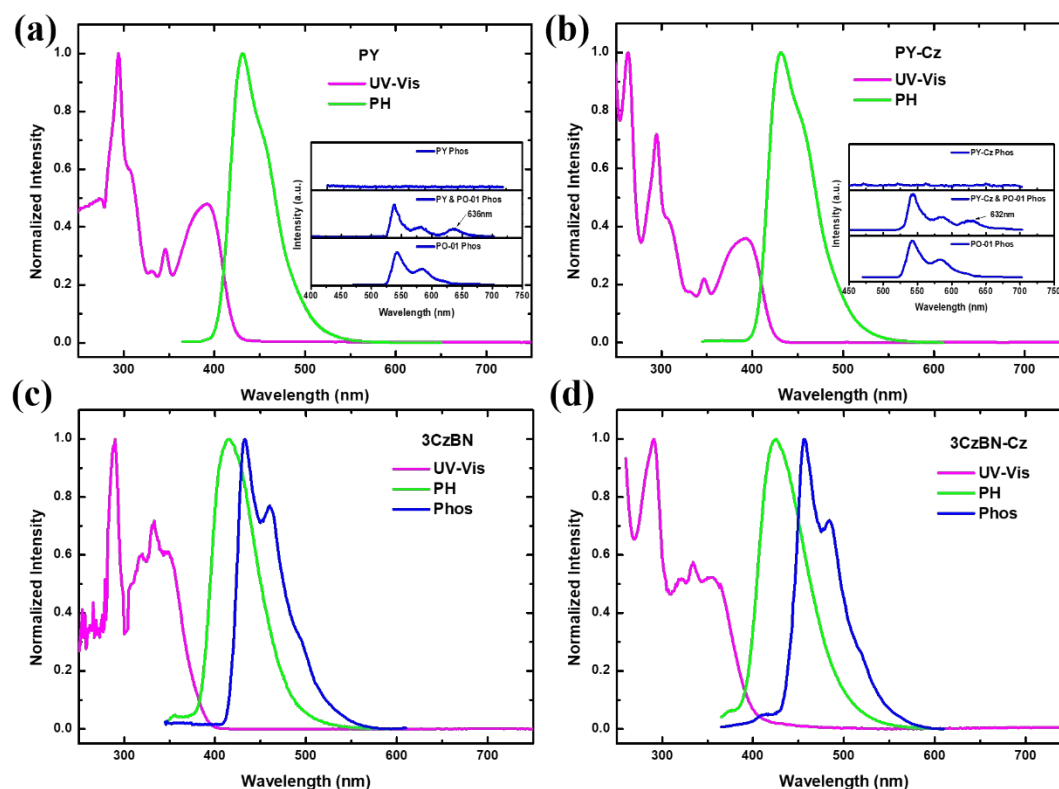


Figure 4 Absorption, fluorescence and phosphorescence spectra of PY (a), PY-Cz (b), 3CzBN (c) and 3CzBN-Cz (d) in toluene, measured in dilute solution with solutes concentration of 1×10^{-5} M, and set 10 ms delayed time for the Phosphorescence spectrum.

that the distance between the centers of mass ($r_{\min} = 16.3 \text{ \AA}$) of 3CzBN-Cz and that of PY-Cz is significantly larger than those ($r_{\min} = 10.6 \text{ \AA}$) between 3CzBN and PY. This means that the Dexter energy transfer is most likely very reduced in the 3CzBN-Cz:PY-Cz blending system. In addition, the number of neighbors in core-dendron blending system is lower for a given distance, indicating that the probability of intermolecular collisions and electron exchange is remarkably reduced. Therefore, the alkyl linked carbazole dendron makes it possible to achieve spatial separation (increased R_{DA}) and reduce the collision probability between the triplet excitons (reduced K_{Dext}).

In addition, the spectral overlap J_{DA} affects the Dexter energy transfer efficiency and the Förster energy efficiency.⁵³

The Förster radius (R_0) can be used to measure the transfer efficiency as:

$$R_0^6 = \frac{9000 \ln(10)}{128 \pi^5 n^4 N_A} \Phi_{PL} K^2 J_{DA}$$

Therefore, the Φ_{PL} of the TADF host and the spectral overlap J_{DA} should be high to achieve effective Förster energy transfer. In conclusion, our calculations suggest that the use of TADF host-sensitized fluorescent emitters and the encapsulation of cores can break the 25% IQE and maximally utilize excitons via efficient Förster transfer rather than Dexter transfer.

2.4 Photophysics Properties

Table 1 Basic photophysical and electrochemical parameters of PY, PY-Cz, 3CzBN and 3CzBN-Cz.

Materials	T_d, T_g [°C]	λ_{abs} [nm] ^a	λ_{em} [nm] ^b	E_g [eV] ^c	S_1/T_1 [eV] ^{d,e}	ΔE_{st} [eV] ^f	HOMO [eV] ^g	LUMO [eV] ^h
PY	385,113	346, 391	431	2.94	3.08/1.95	1.13	-5.47	-2.53
PY-Cz	413,82	346, 392	431	2.94	3.06/1.96	1.10	-5.50	-2.56
3CzBN	401,117	331, 348	415	3.19	3.20/2.87	0.23	-5.75	-2.56
3CzBN-Cz	432,85	333, 354	423	3.10	3.18/2.88	0.30	-5.74	-2.64

a) Measured in toluene solution at 300 K. b) Measured in toluene solution at 300 K. c) Estimated from the absorption edges in toluene. d) Calculated from the onset of the fluorescence spectra in toluene at 300 K. e) Estimated from onset of the phosphorescence spectra in toluene at 77 K. f) The difference between S_1 energy and T_1 energy. g) Determined by the CV measurement. h) Calculated from the energy gap and HOMO.

The UV-Visible absorption and photoluminescence (PL) spectra of the materials were measured (Figure 4 and Figure S5). Intense absorption bands were observed in toluene for all materials. The lowest absorption bands of PY and PY-Cz are located at 395 nm, which is ascribed to the $\pi-\pi^*$ transitions of pyrene. The emission band peaks at 431 nm are attributed to vibronic structures. The absorption and emission spectra show a good mirror-image relationship. 3CzBN and 3CzBN-Cz have a

intensity when water fraction increased gradually from 0% to 100%. The decrease is due to the formation of aggregates from ACQ. When PY was encapsulated with alkyl chain linked carbazole (PY-Cz), the ACQ was suppressed to a certain extent. At the same concentration of 1×10^{-5} M, PY-Cz shows a stronger photoluminescence intensity than PY, as shown in Figure 5b. Therefore, the dendrimer structure can suppress molecular stacking and emission quenching because of the peripheral

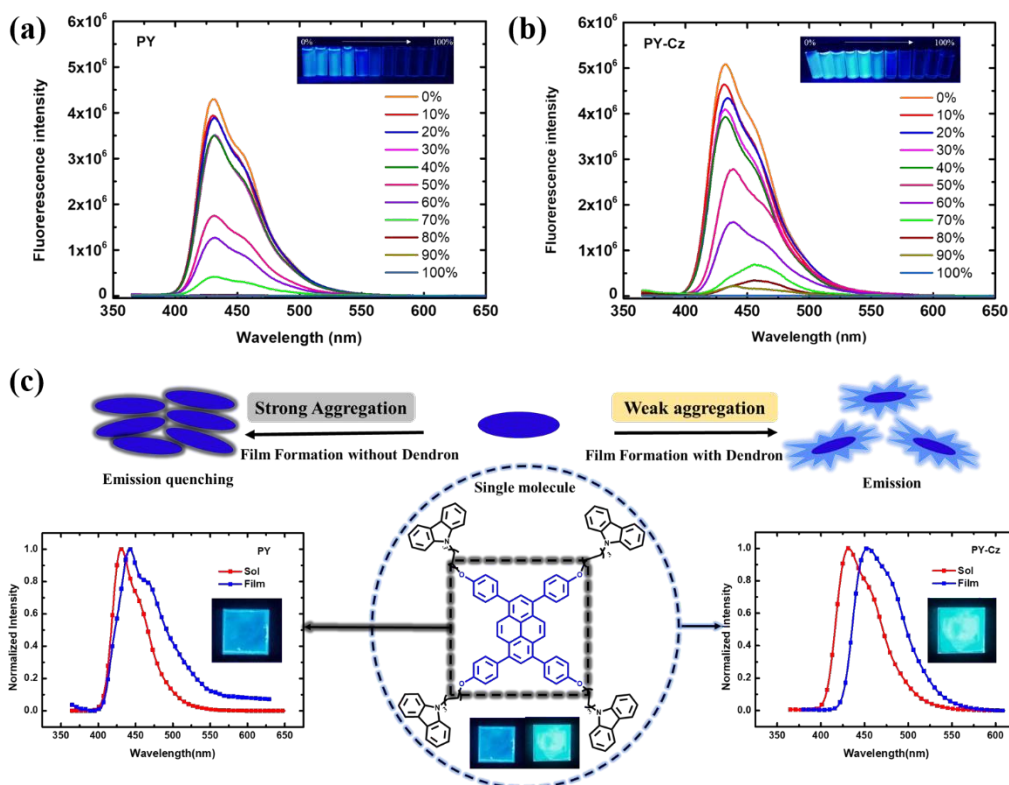


Figure 5 Fluorescence spectra of PY (a) and PY-Cz (b) (10^{-5} M) in tetrahydrofuran and water mixtures with the volume fractions of water are 0%, 10%, 20%, 30%, 40%, 50%, 60%, 70%, 80%, 90%, 100% (Fluorescence images of PY upon excitation with 365 nm light source). (c) Schematic diagram of film emission in the presence and absence of stacking. PL spectra of PY (left) and PY-Cz (right) in solution (10^{-5} mol L $^{-1}$ in CH $_2$ Cl $_2$) and in neat film.

lowest absorption band around 360 nm due to the $\pi-\pi^*$ transitions of carbazoles. The phosphorescence spectra at 77K were measured in toluene to obtain T_1 energy. For PY and PY-Cz, no long-lived phosphorescence emission was directly observed after 10 ms. This suggests that the intersystem crossing (ISC) rate from S_1 to T_1 may be much lower than the radiative rate of S_1 , which leads to an invisible phosphorescence spectrum. We further attempted to sensitize the T_1 state using the PO-01 phosphorescent dye with a low E_{T_1} of 2.30 eV. New emission peaks at 636 nm and 632 nm were observed in the delayed phosphorescence spectrum. They were assigned to the T_1 state of PY and PY-Cz. The measurements clearly showed the existence of much lower T_1 energy levels of 1.95 eV and 1.96 eV for PY and PY-Cz, respectively. Then ΔE_{st} values were calculated as 1.13 eV and 1.10 eV. In addition, traditional blue fluorescent materials knowingly always suffer from serious aggregation-caused quenching (ACQ) due to conjugated structure and $\pi-\pi^*$ stacking. Figure 5 shows that PY also had a strong emission in diluted tetrahydrofuran (THF) with a significantly decreasing

carbazole shield. It is even more pronounced in the film state (Figure 5c). PY showed PL quenching caused by intermolecular interactions in the film state, and PY-Cz showed improved PL intensity because of the disruption of intermolecular stacking from the substitution of the bulky side groups on the PY core. The photoluminescence quantum yield (PLQY) measured provided further evidence of the enhanced PL. In the film states, PY-Cz had a high PLQY of 86% significantly higher than for PY (32%). Apart from the improved PLQY, the spectral overlap between the host and these molecules is also important for the TSF system. The TADF host materials 3CzBN and 3CzBN-Cz were designed and synthesized to sensitize PY and PY-Cz, respectively. Figure S5 shows that 3CzBN-Cz had a deeper emission peak (435 nm) than 3CzBN (450nm) due to restricted molecular aggregation in neat film state. It was also reported adding the carbazole dendrons enhances the PLQY of the TADF materials. The PLQY of the 3CzBN and 3CzBN-Cz films were 45% and 63%, respectively. In addition, UV-Visible absorption spectra of the PY-Cz film and the PL spectra of the 3CzBN-Cz film exhibit a larger spectral overlap between the

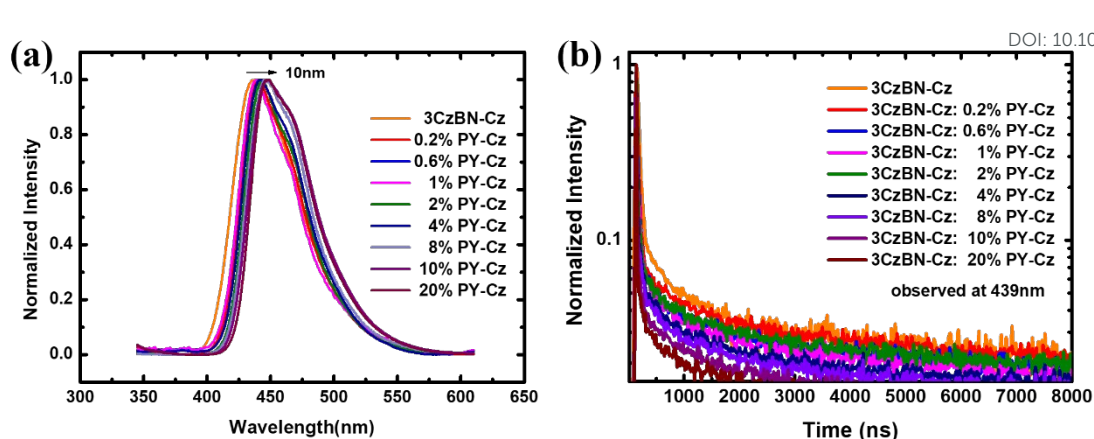


Figure 6 (a) The PL spectra of the 3CzBN-Cz:PY-Cz films. (b) The transient PL decay curves of the 3CzBN-Cz:PY-Cz films observed at 439 nm.

donor emission spectrum and the acceptor absorption spectrum. From the integration of the emission and absorption spectra, 3CzBN-Cz had the larger J_{DA} (0.18) than 3CzBN (0.12), along with a deeper emission peak at 439 nm (shown in Figure S5). It confirms that encapsulation of fluorescence cores improved the PLQY and the energy Förster transfer efficiency.

The time-resolved photoluminescence spectra and the PLQY in the film state were measured to further confirm the

enhancement of the Förster energy transfer and demonstrate the TADF properties of 3CzBN-Cz. In the presence of oxygen, 3CzBN and 3CzBN-Cz possess short lifetimes at the scale of tens of nanoseconds. However, after deoxygenation of the solutions by bubbling nitrogen, the delayed PL decay components are observed for these compounds, which imply that the triplet excitons of the emitters are involved in the radiative decay process. The values of PLQY, the prompt and delayed lifetimes and kinetic parameters including the

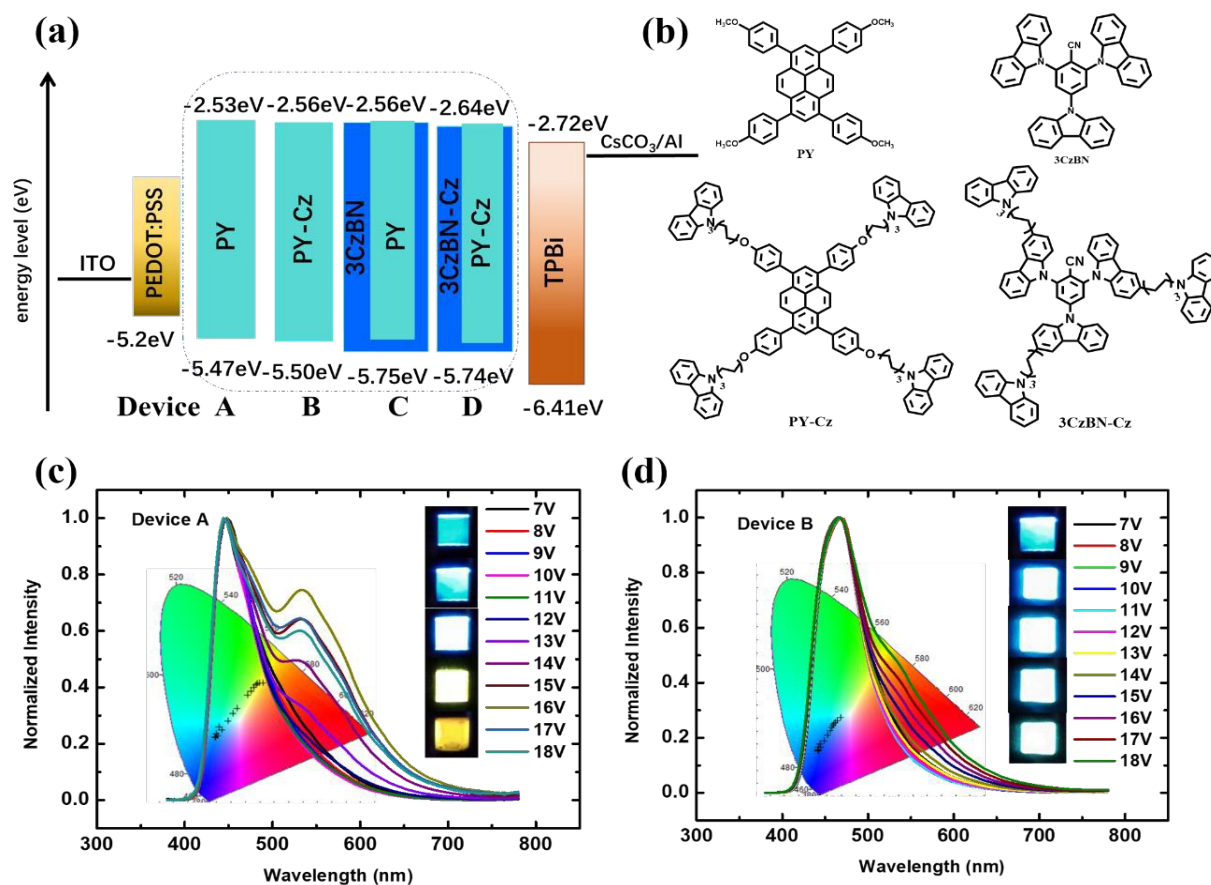


Figure 7 (a) Energy-level arrangement of the organic layers in the OLEDs devices. (b) Chemical structures of the organic materials used in the OLED devices (c) The EL spectra of Device A from 7V to 18V (Inset: the CIE of Device A in different voltage). (d) The EL spectra of Device B from 7V to 18V (Inset: the CIE of Device A in different voltage).

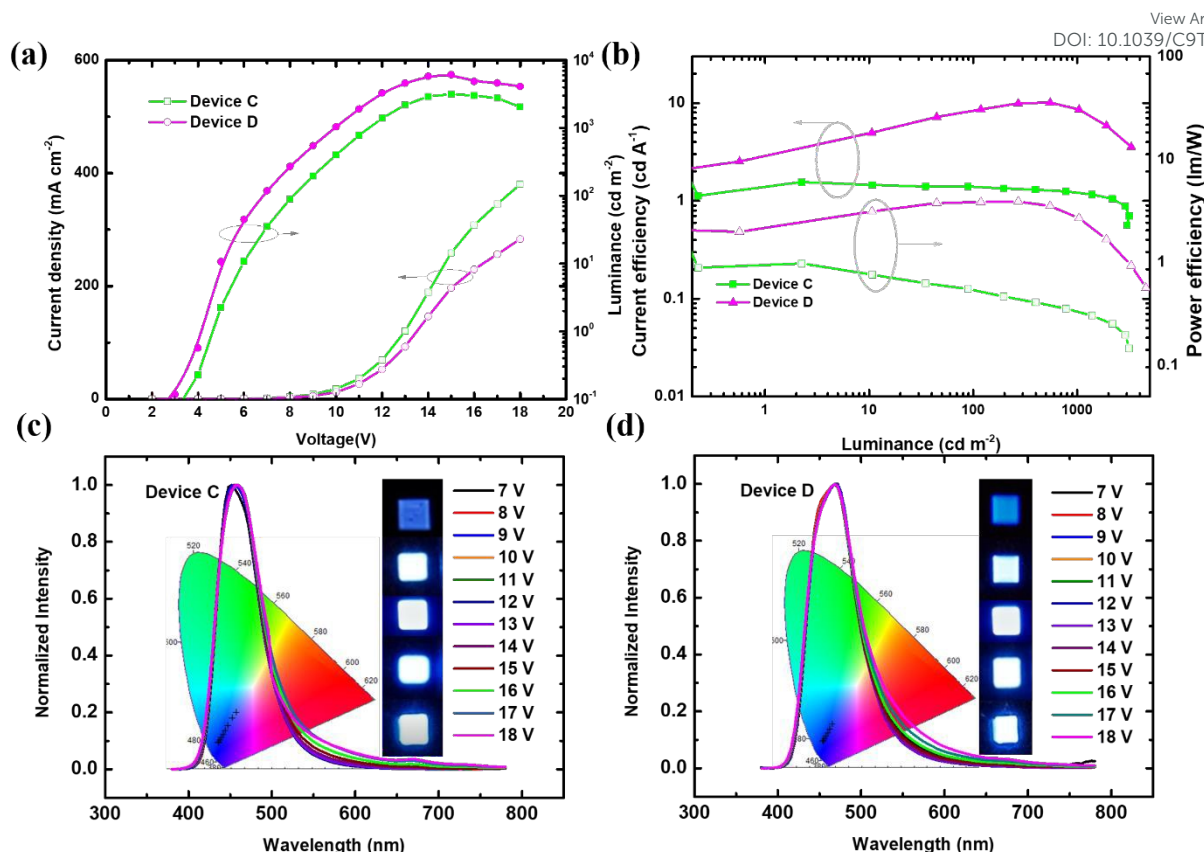


Figure 8 (a) Current density-voltage-luminance (J-V-L) characteristics; (b) Current efficiencies and power efficiencies versus luminance plots. (c) The EL spectra of Device C in different voltage. (d) The EL spectra of Device B in different voltage.

radiative decay rate are summarized in Table S2. Because of the encapsulation effect by the peripheral carbazole, the lifetime of 3CzBN-Cz is 2.3 μ s and is larger than that of 3CzBN (1.8 μ s). Figure 6 and Figure S6 shows the evolution of PL spectra of 3CzBN: PY and 3CzBN-Cz:PY-Cz with the doping concentration. When the doping concentration increases, the PL emission intensity of 3CzBN-Cz gradually decreases and the PL emission of PY-Cz with the vibrational structure appears. This is especially clear for a doping concentration of 8% where the fluorescent shoulder peak of PY-Cz increased, which indicates the efficient energy transfer from the host to the dopant. A similar trend was also observed in the 3CzBN: PY film (Figure S6). The PLQY of the 3CzBN:PY film first increases from 0.30 to 0.52, then decrease to 0.43 with the increasing doping rate. The optimal doping concentration is 10%. Similarly, by applying CDS, the best doping concentration for 3CzBN-Cz:PY-Cz is 10%, which corresponds to a maximum PLQY value of 0.87. The prompt and delayed photoluminescence spectra of the doped films were also measured to investigate the energy transfer process. The delay component of the 3CzBN: PY and 3CzBN-Cz: PY-Cz photoluminescence decay curves gradually when the doping concentration increased. This indicates that the energy can efficiently transfer from the TADF hosts to the fluorescent dopants by Förster energy transfer.⁴⁵ As a result, the encapsulation of the host and the guest facilitates the efficient energy-transfer and yields a high PLQY, which is useful for the optimization of the device efficiency.

2.5 Electroluminescent Properties

Given the efficient Förster energy transfer obtained, the performance of devices with self-encapsulation materials was measured. The solution-processed OLED devices were fabricated using the device structure of ITO/PEDOT:PSS(40nm)/EML(60nm)/TPBI(40nm)/Cs₂CO₃(2nm)/Al, as shown in Figure 7. First, non-doped devices using pristine films were fabricated and characterized. Figure 7c shows the electroluminescent (EL) spectra of devices using PY that exhibit additional emissions at longer wavelengths, which were attributed to the excimer formed by the excited and ground states of the PY molecule. The intensity of emission at longer wavelength gradually increased with the driving voltage. The emission color depends on the driving voltage and changes from deep blue to yellow. After encapsulation by alkyl chained carbazoles, the EL spectra of PY-Cz only showed a slight emission at longer wavelengths (Figure 7d). Although the excimer still exists, the intensity of the excimer emission was effectively suppressed, which fully demonstrates that the molecular aggregation and the formation of excimers were significantly reduced in the encapsulated system. Furthermore, the performance of the device using PY-Cz was also improved with an increased luminance and a higher efficiency, as shown in Figure S7. It indicates that exciton utilization efficiency was improved and that exciton quenching was suppressed from

Table 2 Device performances of the solution-processed OLEDs based on PY, PY-Cz, 3CzBN:PY, 3CzBN-Cz:PY-Cz emissive layer.

Device	emitter	V_{on}^a	EL(nm)	CE_{max}^b	PE_{max}^c	EQE_{max}^d	CE^e	L_{max}^f	$CIE(x,y)^g$
A	PY	6.3	450, 532	0.26	0.07	0.23	0.14/0.20	1000	(0.21,0.28)
B	PY-Cz	4.0	472	1.05	0.52	0.96	0.99/0.85	1500	(0.16,0.17)
C	3CzBN:PY	4.5	460	2.71	1.70	2.02	2.40/2.12	3200	(0.16,0.13)
D	3CzBN-Cz:PY-Cz	4.1	468	13.92	7.60	10.16	12.40/8.61	6200	(0.15,0.14)

^a V_{on} = turn-on voltage at 1 cd m^{-2} , ^b CE_{max} = maximum current efficiency, ^c PE_{max} = maximum power efficiency, ^d EQE_{max} = maximum external quantum efficiency, ^eCurrent efficiency at the luminance of 100 cd m^{-2} , 1000 cd m^{-2} , ^f L_{max} = maximum luminance, ^gCIE = the Commission Internationale de L'Eclairage coordinates at 10 V

the effect of the peripheral carbazole branches. Even so, the exciton utilization is only 25% under electric excitation because the other 75% excitons are injected into the triplet state of the traditional fluorophore and radiation transition is forbidden.

To verify the better performance of the TADF dendrimer in the doped device, two types of devices with different emitting layers (EMLs) were compared: (C) 3CzBN: PY and (D) 3CzBN-Cz:PY-Cz. The optimized doping concentrations of the EML was 10 wt%. Figure 8 shows the emission from the PY-Cz (PY) dopant in the EL spectra and the low hardly visible emission from 3CzBN-Cz (3CzBN), which indicates the complete energy transfer from the host to the guest. In addition, excimer formation is prevented and the emission at longer wavelength disappears in the TSF system, especially in the optimized system using encapsulated materials. The 3CzBN-Cz:PY-Cz based device exhibited an improved color purity with Commission International de l'Eclairage (CIE) coordinates of (0.15, 0.14) due to the reduced host-host and host-guest intermolecular interactions. Figure 8 shows that the performance of Device C based on 3CzBN:PY emissive layer and Device D using the 3CzBN-Cz:PY-Cz emissive layer. Device C exhibits a maximum luminance of current efficiency (CE) of 2.71 cd/A and external quantum efficiency (EQE) of 2.06%. They are higher than for Device A due to triplet harvesting through the TADF process. Encouragingly, by applying CDS, the EQE of Device D is above 5-fold higher than those of Device C. This further confirms the efficient Forster energy transfer through the spatial separation of the TADF hosts and the fluorescent guests, and that the energy loss via TTA, TPA of host-host interaction, and host-guest interaction quenching is efficiently blocked. A cascade energy transfer channel formed in Device D due to high-bandgap carbazole branches, and excitons can flow to the low-energy fluorescent cores and radiate light. Meanwhile the FWHM of the devices based on optimized TSF system is only 65 nm for driving voltage within 7-18 V. It is narrower than for the devices using TADF materials (typically 80-120 nm).⁵⁴ This shows the superiority of the optimized TADF-sensitized fluorescence system.

Conclusions

In summary, we have demonstrated a novel technique to improve the efficiency of fluorescent OLEDs. By combining core-dendron system and TADF-sensitized fluorescence system, Förster energy-transfer from the host to the guest was efficiently enhanced whereas Dexter energy transfer was suppressed by spatially separating the fluorescent guest and the TADF host. Because of the suppressed short-range electron exchange, the triplet-triplet annihilation of the fluorescent guest is blocked and the resulting deep-blue OLEDs had high external quantum efficiency of 10.16% with a stable color purity (FWHM = 65 nm). Our work provides a practical strategy to develop high efficient deep blue emitters, and highly-efficient deep blue OLEDs when TADF dendrimers with a smaller ΔE_{ST} are combined with hyper-fluorescent dendrimers.

Conflicts of interest

There are no conflicts to declare.

Acknowledgements

We are grateful for the grants from the National Natural Science Foundation of China (21875036 and 51103023), the Fundamental Research Funds for the Central Universities (2242016K41082), We are also thankful for the National Basic Research Program (973 program, 2013CB932902), the Priority Academic Program Development of Jiangsu Higher Education Institutions, Nanjing science and technology committee (2014-030002).

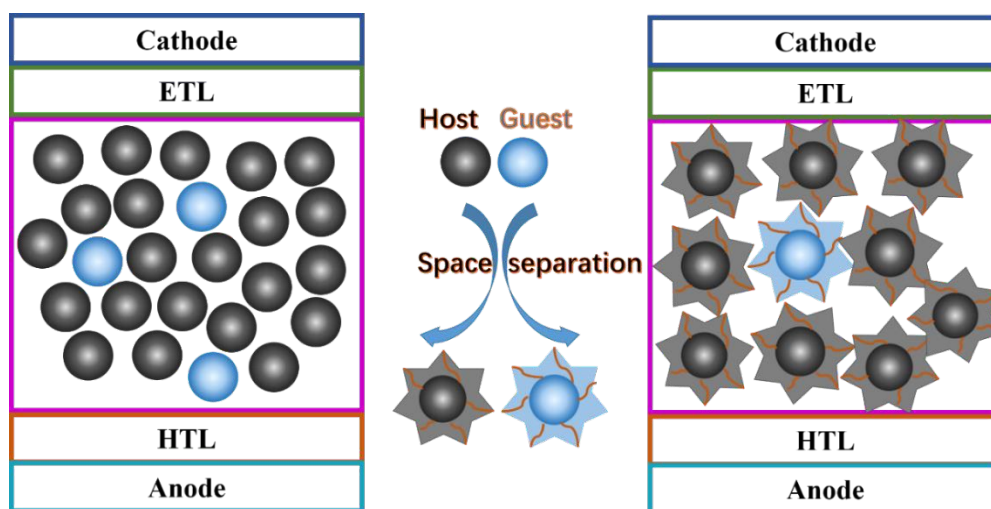
Notes and references

- H. Uoyama, K. Goushi, K. Shizu, H. Nomura and C. Adachi, *Nature*, 2012, **492**, 234.
- Y. Zou, S. Gong, G. Xie and C. Yang, *Adv. Opt. Mater.*, 2018, **6**, 1800568.
- M. Y. Wong and E. Zysman-Colman, *Adv. Mater.*, 2017, **29**, 1605444.
- Y. Yang, Q. Zhao, W. Feng and F. Li, *Chem. Rev.*, 2013, **113**, 192-270.
- T. D. Ashton, K. A. Jolliffe and F. M. Pfeffer, *Chem. Soc. Rev.*, 2015, **44**, 4547.
- K. Li and B. Liu. *Chem. Soc. Rev.*, 2014, **43**, 6570.
- J. B. Birks. *Wiley-Interscience*, London, 1970.

- 8 S. A. Jenekhe and J. A. Osaheni, *Science*, 1994, **265**, 765.
- 9 Y. Hong, J. W. Y. Lam and B. Z. Tang, *Chem. Soc. Rev.*, 2011, **40**, 5361.
- 10 C. L. Chiang, S. M. Tseng, C. T. Chen, C.P. Hsu and C.F. Shu, *Adv. Funct. Mater.*, 2008, **18**, 248.
- 11 J. S. Yang and J. L. Yan, *Chem. Commun.*, 2008, **13**, 1501.
- 12 B. S. Gaylord, S. Wang, A. J. Heeger and G. C. Bazan, *J. Am. Chem. Soc.*, 2001, **123**, 6417.
- 13 V. Bulovic, A. Shoustikov, M. A. Baldo, E. Bose, V. G. Kozlov, M. E. Thompson and S. R. Forrest, *Chem. Phys. Lett.*, 1998, **287**, 455.
- 14 A. C. Grimsdale, K. L. Chan, R. E. Martin and P. G. Jokisz, *Chem. Rev.*, 2009, **109**, 897.
- 15 Y. Hong, J. W. Y. Lam and B. Z. Tang, *Chem. Commun.*, 2009, **29**, 4332.
- 16 S. Y. Byeon, S. H. Han and J. Y. Lee, *Adv. Opt. Mater.*, 2018, **6**, 1701263.
- 17 C.-Y. Chan, L.-S. Cui, J. U. Kim, H. Nakanotani and C. Adachi, *Adv. Funct. Mater.*, 2018, **28**, 1706023.
- 18 J. Luo, Z. Xie, J. W. Y. Lam, L. Cheng, H. Y. Chen, C. F. Qiu, H. S. Kwok, X. W. Zhan, Y. Q. Liu, D. B. Zhu and B. Z. Tang, *Chem. Commun.*, 2001, **18**, 1740.
- 19 S. Kim, B. Kim, J. Lee, H. Shin, Y.-I. Park and J. Park, *Mater. Sci. Eng., R*, 2016, **99**, 1.
- 20 Z. Zhao, S. Chen, X. Shen, F. Mahtab, Y. Yu, P. Lu, J. W. Lam, H. S. Kwok and B. Z. Tang, *Chem. Commun.*, 2010, **46**, 686.
- 21 M. Gao, H. Su, Y. Lin, X. Ling, S. Li, A. Qin and B. Z. Tang, *Chem. Sci.*, 2017, **8**, 1763.
- 22 J. Guo, S. Hu, W. Luo, R. Hu, A. Qin, Z. Zhao and B. Z. Tang, *Chem. Commun.*, 2017, **53**, 1463.
- 23 J. Guo, X.-L. Li, H. Nie, W. Luo, R. Hu, A. Qin, Z. Zhao, S.-J. Su and B. Z. Tang, *Chem. Mater.*, 2017, **29**, 3623.
- 24 J. Huang, H. Nie, J. Zeng, Z. Zhuang, S. Gan, Y. Cai, J. Guo, S. J. Su, Z. Zhao and B. Z. Tang, *Angew. Chem., Int. Ed.*, 2017, **56**, 12971.
- 25 L. Viglianti, N. L. C. Leung, N. Xie, X. Gu, H. H. Y. Sung, Q. Miao, I. D. Williams, E. Licandro and B. Z. Tang, *Chem. Sci.*, 2017, **8**, 2629.
- 26 H. Park, J. Lee, I. Kang, H.Y. Chu, J. I. Lee, S.K. Kwon and Y.H. Kim, *J. Mater. Chem.* **22**, 2695.
- 27 Z.Q. Wang, C. Xu, W.Z. Wang, L.M. Duan, Z. Li and B.T. Zhao, B.M. Ji, N. J. Chem. 2015, **36**, 662.
- 28 M.S. Gong, H.S. Lee and Y. M. Jeon, *J. Mater. Chem.* 2010, **20**, 10735.
- 29 C. H. Wu, C. H. Chien, F. M. Hsu, P. I. Shih and C. F. Shu, *J. Mater. Chem.* 2009, **19**, 1464.
- 30 S. L. Lai, Q. X. Tong, M. Y. Chan, T. W. Ng, M. F. Lo, S.T. Lee and C. S. Lee, *J. Mater. Chem.* 2011, **21**, 1206.
- 31 T. M. Figueira-Duarte, P. G. D. Rosso, R. Trättnig, S. Sax, E. J. W. List and K. Mullen, *Adv. Mater.* 2010, **22**, 990.
- 32 N. G. Valsange, F. L. Wong, D. Shinde, C. S. Lee, V. A. L. Roy, S. Manzhos, K. Feron, S. Chang, R. Katoh, P. Sonar and P. P. Wadgaonkar, *New J. Chem.*, 2017, **41**, 11383.
- 33 X. Ban, A. Zhu, T. Zhang, Z. Tong, W. Jiang and Y. Sun, *ACS Appl. Mater. Interfaces*, 2017, **9**, 21900. View Article Online DOI: 10.1039/C9TC03334C
- 34 Y. Wang, S. Wang, N. Zhao, B. Gao, S. Shao, J. Ding, L. Wang, X. Jing and F. Wang, *Polymer Chemistry*, 2015, **6**, 1180.
- 35 J. Ding, J. Lü, Y. Cheng, Z. Xie, L. Wang, X. Jing and F. Wang, *Adv. Funct. Mater.*, 2008, **18**, 2754.
- 36 Y. Liu, C. Li, Z. Ren, S. Yan and MR. Bryce, *Nat. Rev. Mater.* 2018, **3**, 18020.
- 37 Y. Zou, S. Gong, G. Xie and C. Yang, *Adv. Opt. Mater.* 2018, **6**, 1800568.
- 38 N. J. Turro, V. Ramamurthy and J. C. Scaiano, *Photochem. Photobiol.*, 2012, **88**, 1033
- 39 A. Köhler and H. Bässler, *John Wiley & Sons*, 2015.
- 40 S. H. Han and J. Y. Lee, *J. Mater. Chem. C*, 2018, **6**, 1504.
- 41 S. Y. Byeon, D. R. Lee, K. S. Yook and J. Y. Lee, *Adv. Mater.*, 2019, 1803714.
- 42 D. H. Ahn, J. H. Jeong, J. Song, J. Y. Lee and J. H. Kwon, *ACS Appl. Mater. Interfaces*, 2018, **10**, 10246.
- 43 X. K. Liu, Z. Chen, C. J. Zheng, M. Chen, W. Liu, X. H. Zhang and C. S. Lee, *Adv. Mater.*, 2015, **27**, 2025.
- 44 H. Nakanotani, T. Higuchi, T. Furukawa, K. Masui, K. Morimoto, M. Numata, H. Tanaka, Y. Sagara, T. Yasuda and C. Adachi, *Nat. Commun.*, 2014, **5**, 4016.
- 45 D. Zhang, L. Duan, C. Li, Y. Li, H. Li, D. Zhang and Y. Qiu, *Adv. Mater.*, 2014, **26**, 5050.
- 46 D. Zhang, X. Song, M. Cai and L. Duan, *Adv. Mater.*, 2018, **30**, 1705250.
- 47 T. Lei, J.-Y. Wang and J. Pei, *Chem. Mater.*, 2013, **26**, 594.
- 48 D. Zhang, M. Cai, Z. Bin, Y. Zhang, D. Zhang and L. Duan, *Chem. Sci.*, 2016, **7**, 3355-3363.
- 49 R. A. Marcus, *J. Chem. Phys.*, 1956, **24**, 966.
- 50 R. A. Marcus, *Reviews of Modern Physics*, 1993, **65**, 599.
- 51 C. Tonnele, M. Stroet, B. Caron, A. J. Clulow, R. C. R. Nagiri, A. K. Malde, P. L. Burn, I. R. Gentle, A. E. Mark and B. J. Powell, *Angew. Chem., Int. Ed.*, 2017, **56**, 8402.
- 52 T. Lu, Molclus program; Beijing Kein Research Center for Natural Science, China, 2016; <http://www.keinsci.com/research/molclus.html>.
- 53 W. S. Jeon, T. J. Park, S. Y. Kim, R. Pode, J. Jang and J. H. Kwon, *Org. Electron.*, 2009, **10**, 240.
- 54 X. Liu, Z. Chen, C. Zheng, M. Chen, W. Liu, X. Zhang and C. Lee, *Adv. Mater.*, 2015, **27**, 2025-2030.

Spatial separation of TADF sensitizer and fluorescent emitter improve the energy transfer efficiency by suppressing energy loss and further enhance electroluminescent performance.

Online
DOI: 10.1039/C9TC03334C



TOC